Review Article

Halide-Perovskite-Based Memristor Devices and Their Application in Neuromorphic Computing

Soumitra Satapathi[1,2,*] Kanishka Raj,[1] Yukta,[2] and Mohammad Adil Afroz[2]

[1]*Center of Nanotechnology, Indian Institute of Technology Roorkee, Haridwar, Uttarakhand 247667, India*
[2]*Department of Physics, Indian Institute of Technology Roorkee, Haridwar, Uttarakhand 247667, India*

Advanced intelligent systems, including memristors and neuromorphic devices, that render high speed and consume little power are getting increasing attention due to the limitations of Moore's law and the von Neumann bottleneck. Memristors and transistor-based synaptic devices demonstrate strong potential in neuromorphic computing. Active materials used in high-performance memristors need to show a poor defect-migration barrier and high speed of defect migration. Imperfections in halide perovskites lead to charge trapping and ion migration, and hence, make them potential candidates, among other materials, to be used to fabricate synaptic devices. Metal-halide-perovskite-based artificial synaptic devices are successful in emulating synaptic plasticity and the learning function of the human brain. In this article, the structure, mechanism, and properties of memristors are discussed first, followed by a discussion on recent advancements in halide-perovskite-based memristors and artificial synaptic devices with different configurations (two-terminals and three-terminals) stimulated by light or an electric pulse. Finally, the future opportunities and challenges in the field are presented briefly.

I. INTRODUCTION

In the last decade, halide perovskites (HPs) have gained increased attention for use in different optoelectronic devices. The use of HPs in solar cells has enabled a power conversion efficiency exceeding 25% owing to their fascinating properties, such as high absorption coefficients, tunable band gaps, high charge-carrier mobility, and long carrier-diffusion lengths [1–5]. These exceptional properties also enable their utilization in other optoelectronic devices like light-emitting diodes, photodetectors, transistors [6–9], and resistive-switching (RS) memories [10,11]. The exceptional properties of HPs, such as mixed ionic-electronic conduction behavior, adjustable band gaps, low operating currents, and ultralow leakage currents, give HPs the potential to be used in memristors and artificial synaptic devices [12–14].

Memristors, also known as resistive random access memory (RRAM), are the most prominent candidate in the direction of next-generation memory technology due to their multiple advantageous properties, such as high integration density, low operation energy, and high switching speed. It can be used as the main memory and working memory. As the main memory, it acts as a nonvolatile memory and stores an enormous amount of data. Its write-to-erase ratio is very high as working memory, and power consumption is very low. Memristors have massive potential in next-generation smart electronics and neuromorphic computing-based appliances [15,16]. The memristor, often referred to as RS memory, was postulated in 1971 by Chua as a fourth circuit element, the first three being resistor, capacitor, and inductor [17]. Hewlett-Packard labs fabricated a memristor in 2008 by sandwiching titanium dioxide in between two metal contacts. Titanium dioxide has two regions attached in series. The first region has a high dopant concentration and low resistance, and the second region has a low dopant concentration with high resistance. When the voltage was applied to the device, researchers observed a change in total resistance of the device. However, when a sine-wave voltage is applied to the device, the *I*-*V* curve of the device forms a structure similar to "8," which confirms the bipolar switching behavior of the memristive device [18,19]. The memristor's resistance depends on the current and voltage history; therefore, it can retain data, even after removal of power. It has many promising properties like low power consumption, fast switching speed, high durability, long retention time, fine miniaturization, three-dimensional (3D) stacking, and structural simplicity. Its compatibility with semiconductor devices makes it a promising component for next-generation smart devices, mass memory storage, internet of things, neuromorphic computing, and artificial synapses (which intend to emulate the structure and function of the human brain at the circuitry level) [20]. Numerous materials are used

*soumitra.satapathi@ph.iitr.ac.in

as an insulating layer in memristors, such as metal oxides [21,22], organic materials [23–26], chalcogenides [27,28], amorphous carbon [29,30], and amorphous silicon [31,32]. The HP has recently been utilized in memristors, and they benefit from the ionic-electronic conductivity [33,34]. Precisely, distinctive functions can be established with HP-based memristors, taking advantage of their excellent light-absorption ability coupled with electronic and ionic processes [35].

The human brain occupies 2 l of space with a weight ratio of 2% in the human body, and it is composed of around 10^{11} neurons connected by 10^{15} synapses. The human brain acts as a control center for the nervous system, which rapidly processes a large amount of information in parallel while consuming low power of around 1–100 fJ per synaptic event [36–38]. Figure 1(a) illustrates biological synapses, including the presynaptic membrane, postsynaptic membrane, and synaptic cleft. A synapse acts as a junction that transfers electrical impulse signals between two nerve cells (pre- and postneurons). When a preneuron receives electrical signals, neurotransmitters are generated in a synaptic vesicle. A Ca^{2+} channel in the preneuron then opens, resulting in an influx of Ca^{2+} ions, which further leads to emission of the synaptic vesicle to the synaptic cleft and the vesicle binds receptor molecules at the postsynaptic membrane. This follows the transmission of an electrical signal from a preneuron to a postneuron. Neuromorphic computing is the process of computing utilizing a machine that comprises many simple processors or memory structures (e.g., neurons and synapses) and communicates with simple messages (e.g., spikes). Neuromorphic computing combines information processing and remembering. Two-terminal memristors or three-terminal transistors are being considered as promising candidates for artificial synapses due to their ability to emulate the functions of biological synapses owing to their similar transmission characteristics. The artificial synapses are fundamental functional units for neuromorphic computing. An artificial synapse requires the transmission of electrical stimuli from the preneuron to the postneuron. In a memristor, one of metal electrodes acts as a preneuron, the insulating layer as a synapse, and another metal electrode act as a postneuron.

Earlier, Bian *et al.* discussed in detail electronic, photonic, and magnetic stimuli and different architectures of memristor devices. Subsequently, they described the various operating mechanisms, including the conductive filament mechanism, phase-change mechanism, ion migration, carrier trapping-detrapping responsible for synaptic transmission, and resistive switching in various materials. They conclusively narrowed down the different possible obstacles in diverse materials, such as an in-depth understanding of the switching mechanism, device instability and reproducibility, and excessive energy consumption

due to the sneak-path current in crossbar array memristors, which limit the ability of various semiconducting materials to fully mimic biological synapses [42]. Furthermore, Raifuku *et al.* focused on organic-inorganic halide perovskite (OIHP) active-layer-based memristor devices. They explained the detailed working mechanism, device architecture, applications, and recent advances in OIHP-based neuromorphic devices. Ion migration, charge-carrier trapping-detrapping, and photoresponse are a few common mechanisms used in perovskite neuromorphic devices. In ion migration, temperature or an electric field primarily lead to drifting of the mobile ions between opposite electrodes to form a conductive filament (CF) and achieve effective resistive switching from the perovskite materials [43]. On the other hand, space-charge-limited conduction (SCLC) causes the trapping-detrapping of charge carriers that further produces the space electric field and creates the RS effect. In phototunability, the hot carriers are trapped between the active perovskite layer and consecutive electrodes due to the energy-level difference in photosensitized memory devices. Furthermore, Kim *et al.* investigated in detail halide-perovskite-based RRAM devices, their operating mechanism, the classification of the perovskite active layers, and their advantages over conventional RRAM devices. They conclude that halide perovskites are viable materials for RRAM devices owing to their superior *on*:*off* ratio and resistive transition at relatively low operating voltages, but to achieve commercialization an enhancement of the material stability and switching properties is required [44]. Subsequently, Chen *et al.* also focused on the halide-perovskite-active-layer-based artificial synaptic devices. They conclude that the two-terminal- (2T) architecture-based perovskite synaptic devices mainly operate through ion-migration and carrier-trapping mechanisms and can successfully realize the main forms of synaptic functions, including excitatory postsynaptic current (EPSC), short-term potentiation (STP), paired-pulse facilitation (PPF), spike-timing-dependent plasticity (STDP), long-term potentiation (LTP), and spike-rate-dependent plasticity (SRDP) with minimal energy consumption (approximately 20 fJ per synaptic event). Also, the organic-cation-based [methylammonium (MA) or formamidinium (FA)] halide perovskites show better synaptic performance and low energy consumption in comparison to all-inorganic Cs halide perovskites. They also explain the mechanism of vacancy-mediated ion drift diffusion and propose mixed ionic-electronic conduction in perovskite synaptic devices. Furthermore, three-terminal- (3T) architecture-based perovskite synaptic device structures basically resemble the transistor architecture, in which gate electrodes act as a presynaptic membrane that receives external stimuli and the conduction channel is considered to be the postsynaptic membrane. However, the 3T devices show flexible
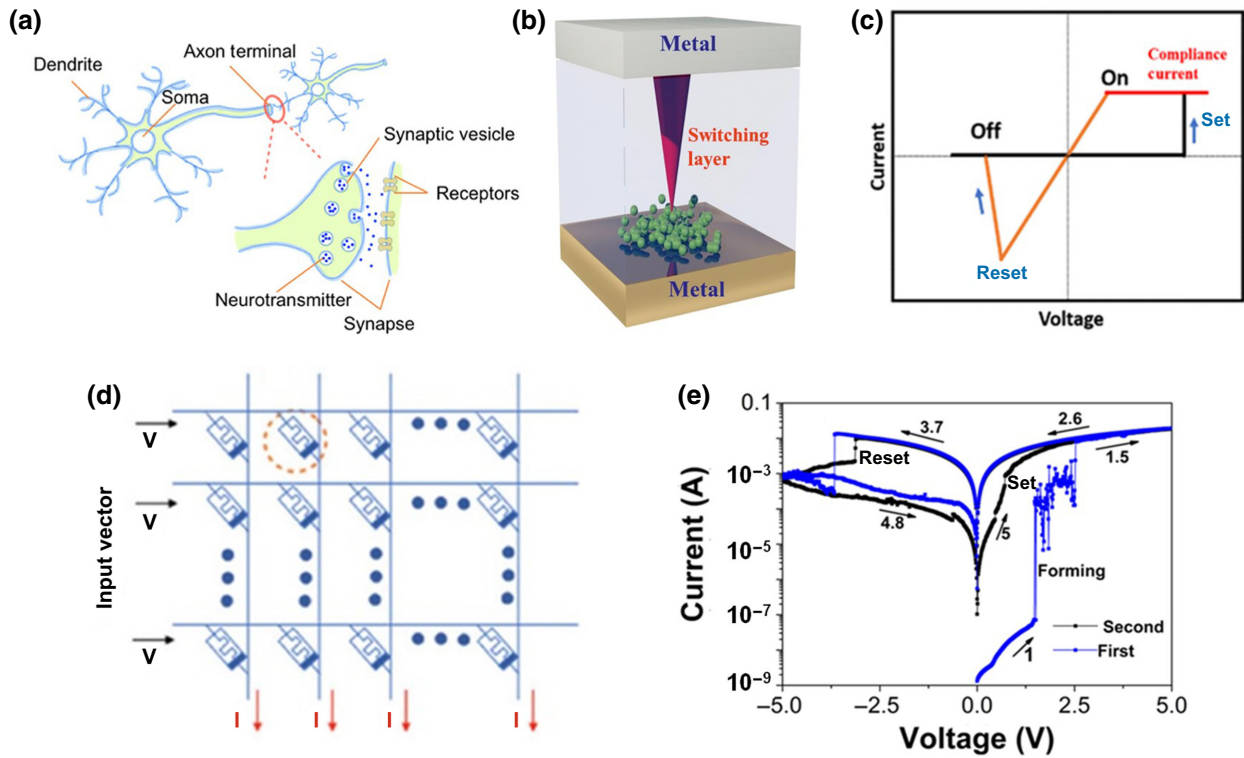
FIG. 1. (a) Schematic of biological synapses. Adapted with permission from Ref. [39]. Copyright (2020) American Chemical Society. (b) Cross-section view of a memristor device. Reprinted from Ref. [40]. Copyright (2016), with permission from Elsevier. (c) *I-V* characteristics and set-reset mechanism of a memristor with bipolar switching. Reprinted with permission from Ref. [41]. Copyright (2018) Springer Nature. (d) Array structure connecting multiple memristor devices. Adapted with permission from Ref. [39]. Copyright (2020) American Chemical Society. (e) Typical *I-V* characteristics of the first two cycles of a HP-based memristor device showing forming, set, and reset processes. Adapted with permission from Ref. [20]. Distributed under a Creative Commons Attribution 4.0 International (CC BY 4.0).

synaptic weight variation, can be expanded to multiterminal devices, and simulate spatiotemporal logic operations, but the complexity of the device architecture makes their integration difficult on large scales [36,45].

Here, we provide a detailed insight into the working mechanism, operation modes, and device architectures of the memristor devices. We further describe the remarkable properties of halide perovskites that make them ideal for memristor applications, as well as summarize recent advancements in the field of halide-perovskite memristors. Also, the importance of the halide perovskite in neuromorphic computing and artificial synapses is reviewed. Furthermore, the fabrication techniques and performance parameters for HP memristor devices are reviewed. Finally, the review is concluded with the existing challenges and perspectives for the development of next-generation neuromorphic computing devices based on halide perovskites.

II. MECHANISM OF MEMRISTOR DEVICES

Generally, a memristive device has a metal-insulator-metal (*M*-*I*-*M*) structure built vertically. In which the

insulating layer is sandwiched between two metal electrodes. The resistive-switching mechanism of the device can be controlled by applying an electric bias to the two metal electrodes. The vertical structure of the device along with resistive switching is illustrated in Fig. 1(b) [16,37,40].

The primary mechanism of a memristor involves RS, i.e., converting the device from a high-resistance state (HRS) to a low-resistance state (LRS) and vice versa induced by light or electrical stimuli. Figure 1(c) illustrates the current-voltage (*I-V*) characteristics and set-reset mechanism with bipolar switching [41]. Switching at the same polarity voltage is known as unipolar switching, and bipolar switching refers to the switching behavior occurring at different polar voltages. When the device switches from the HRS to the LRS, the process is called the set process, and when the device switches from the LRS to the HRS, the process is called the reset process. This mechanism can be classified as electrochemical metallization (ECM) or the valence-change mechanism (VCM), depending on the material composition, fabrication process, and measurement conditions; however, the VCM is preferred, as it can be scaled down for high-density
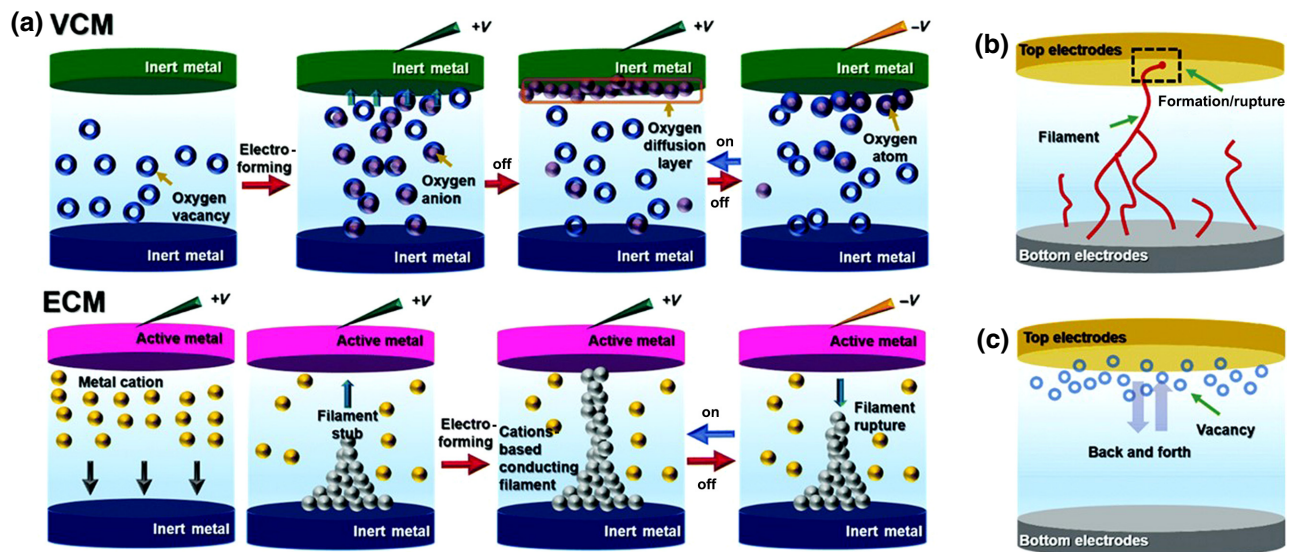
FIG. 2.   (a) Schematics showing the operating mechanism of the resistive-switching behavior, electroforming process, filament formation, and rupture in the switching layer. (b) Filamentary-type switching mechanism and (c) interface-type switching mechanism. (a)–(c) Reprinted with permission from Ref. [44]. Copyright (2019) Royal Society of Chemistry.

integration. Depending on whether RS is discrete or analogous, the memristor can be classified as a digital or analog memristor. A digital memristor is widely being explored as nonvolatile memory, while the analog memristor has enormous possibilities in neuromorphic computing [46]. As a memristor is compatible with the cross-array structure, many memristors connected in microspace can magnify their advantages and enable massively parallel processing as well as have applications in distributed information storage [16,39]. A cross-array structure of a memristor is illustrated in Fig. 1(d).

A. Valence-change mechanism (VCM)

Devices following the VCM are termed anionic devices, as their mechanism majorly depends on the migration of anions under an external field [47]. An insulating layer is sandwiched between the top electrode (TE) and the bottom electrode (BE). In the VCM, when a voltage is applied to the device, anions of the insulating layer migrate, causing vacancy formation in the opposite direction and the CF is formed in the insulating layer by applying sufficiently high voltages followed by a local redox reaction [16,48]. The applied voltage at which the CF forms is referred to as the forming voltage (V_{form}), and the process is known as the forming process [Fig. 1(e)]. The forming process is accomplished before the device enables work, and V_{form} is usually larger than the set and reset voltages [16,20]. In the VCM, when a voltage is applied to the device, anions of the insulating layer migrate, causing vacancy formation in the opposite direction. The vacancy formed leads to the formation of the CF in the insulating layer. The VCM mechanism is illustrated in Fig. 2(a) (upper panel) [44,47].

B. Electrochemical metallization (ECM)

In ECM, an insulating layer is sandwiched between an electrochemically active metal, such as Ag or Cu, and a noble counter electrode, such as Pt, W, or Au. Charged metal cations are released from the active electrode into the memristive layer; these cations migrate and accumulate at the counter electrode after application of an electric field. An electromotive force is generated inside the memristive layer due to the electric field and is termed as nanobattery, which is responsible for the migration of charges. This migration and accumulation of charges depends on the electromotive force, which is governed by external stimuli, such as the ion concentration at the interface and ambient atmosphere. Electrochemical switching depends on the establishment of the CF, which is formed by the mobile cations accumulating in front of the counter electrode. The establishment of the CF is an indispensable initial step and is responsible for the different resistive states: low current before the formation of the CF leads to a HRS and high current after the formation of the CF leads to LRS. As the CF formation eventuates through movement of dissolved metal cations from the active metal interface towards the insulating region, the device following ECM is also called a cationic device. Under the externally applied electric field's influence, dissolved metal cations gravitate towards the inert counter electrode, leaving behind metal vacancies. As metal cations migrate, the insulating layer's effective width reduces, causing the formation of the CF [47]. Figure 2(a) (lower panel) illustrates CF formation and rupture in a device through ECM. The filamentary-type switching mechanism and interface-type switching mechanism are illustrated in Figs. 2(b) and 2(c), respectively.

1. Charge-trapping mechanism

SCLC causes the trapping-detrapping of charge carriers in semiconductors, which further produces the space electric field and creates the RS effect. Also, in defect-prone oxides or hybrid-perovskite materials, the trapping and detrapping of charge carriers through these defect states at the resistive-switching-material– (RSM) electrode interface or in the bulk RSM can induce resistive-switching phenomena [49,50]. In the defect-rich materials, the electrons and holes can be trapped in the interfacial defect states; hence, carrier accumulation results in charge build up, which further modifies the Schottky barrier. The most common analog switching mechanism is considered to be interfacial trapping and is characterized by the evident hysteresis [51,52]. Zawal *et al.* fabricated photoactive memristor devices with a methyl ammonium lead iodide (MAPbI$_3$) perovskite layer sandwiched between two conductive electrodes (ITO and Au). They additionally introduce a carbon nitride (CN) nanoparticle layer into the memristor that exhibits an efficient charge-trapping mechanism in the perovskite memory device. The additional CN nanoparticles provide unique neuromimetic features for the perovskite memristor devices. This significantly lowers the device response time, introduces fading memory or long-term depression features, and subsequently increases the Hebbian learning efficiency [51]. Chen *et al.* also fabricated an artificial photoelectric memristor device based on the carrier trapping-detrapping mechanism. They fabricated a memristor device with core-shell CdSe/ZnS quantum dots and CsPbBr$_3$ perovskite quantum dots. The quantum well structure of CdSe/ZnS quantum dots act as a carrier-trapping center and effectively modulates the resistance of the device. The CdSe/ZnS-CsPbBr$_3$-based memristor device successfully mimics various synaptic functions and can potentially function as a flexible memristor in commercial applications [49].

2. Phase transition

The phase-change process recognized in chalcogenide glass materials serves as the foundation for phase-change RSMs [53]. The electrical resistance of these RSMs changes from low to high, depending upon the phase of the materials. Generally, heating the material above its melting point (joule heating) and inert thermal dissipation are responsible for the crystalline-to-amorphous phase transition in these RSMs [54]. The electrical resistance can be stated as 0 or 1 for data storing for amorphous and crystalline phases, respectively, due to a substantial resistance gap between these states. Other than electrical resistance, the carrier concentration, bonding mechanism, and structural disorder also differ between these two states. In phase-change materials (PCMs), the nanosecond ($\sim$100–1000 ns) timescale is required for the transition from the amorphous-to-crystalline phase

[55,56]. Therefore, to realize efficient resistive switching from PCMs, rapidly crystallizing materials are required. Earlier, Kim *et al.* fabricated oxide perovskite brownmillerite SrFeO$_x$-based memristive devices. They claim that the electrical resistivity of the device changes with a reversible topotactic phase transition between insulating brownmillerite SrFeO$_{2.5}$ to the conducting perovskite, SrFeO$_{3-\delta}$, material. Also, the oxygen-vacancy channel is created to facilitate carrier transport during the phase change over a larger area in between consecutive electrodes. Oxygen-vacancy-channel engineering in the as-designed Au/SrFeO$_{3-\delta}$/SrRuO$_3$/SrTiO$_3$ phase-change memristor devices leads to improved switching performance [57]. Although PCM devices have improved significantly in recent years, there are still several challenges that need to be resolved. Since the transition from the amorphous phase to the crystalline phase takes time, the set switching speed for the PCM is intrinsically slow. Besides, another challenge is the high programming current (reset current, $\leq$100 μA) generated during device operation due to the joule-heating effect. Due to the high reset current in PCM devices, they consume comparatively more power and became incompatible with standard-access devices [57].

3. Dipole alignment

Kiran *et al.* reported negative differential-resistance- (NDR) based resistive switching in vanadyl-phthalocyanine (VOPc) active-layer-based devices with a configuration of ITO/F$_4$TCNQ (2,3,5,6-tetrafluoro-7,7,8,8-tetracyanoquinodimethane)/VOPc/MoO$_3$/Al. In the NDR memristors, the devices are switched from their initial LRS (*on*) to the HRS (*off*) on applying a bias. Here, the *on*-to-*off* state transition is ascribed to the formation and neutralization of interface dipoles at the ITO-VOPc interface. It is concluded that the incorporation of an interface dipole layer (hole- or electron-injection layer) between the switching material and electrode can effectively modulate band alignment (HOMO) and reduce the injection barrier for charge carriers (holes) and leads to low-resistance states in the initial sweep. After formation of the set voltage, the injection barrier would again be altered by the neutralization of dipoles on applying a bias. This further modulates the band structure at the interface and the effective hole-injection barrier is significantly increased and switched to the high-resistance state [58]. Similarly, Whitcher *et al.* also successfully realized resistive switching in ITO/poly(9-vinylcarbazole) (PVK)/Al-structured devices due to interfacial dipole alignment and the band-bending phenomena occurring between ITO-PVK and PVK-Al interfaces [59]. Most recently, Schranghamer *et al.* demonstrated that various synaptic functions were realized in graphene memristors based on dipole-moment switching [60].

4. Ferroelectric tunnel junctions

In ferroelectric tunnel-junction (FTJ) memory theory, the information is encrypted by the polarization orientation in a transparent tunneling ferroelectric barrier material, embedded between two consecutive electrodes [61,62]. The synaptic process emulated by the FTJ consumes a very low amount of energy due to the small values of the tunneling current. A memristor response is produced in a FTJ by the progressive reversal of ferroelectric polarization inside a narrow tunnel barrier and the resulting changes in the potential barrier generated by electrostatic charge screening [63]. A change in polarization (switching) has an effect on the asymmetric potential-energy profile and, consequently, changes the tunneling current through the barrier. The resistance levels can be changed between low and high states (*on* and *off*, respectively) in the ferroelectric layer by switching the polarization of the material [62,64]. Earlier, FTJs were engineered by using standard ferroelectric perovskite materials. Subsequentially, the detection of the ferroelectric characteristics in doped polycrystalline hafnium oxide thin and ultrathin films provides an opportunity to construct ferroelectric memory devices that are compatible with complementary metal oxide semiconductor (CMOS) technology. Furthermore, in ferroelectrics, the domain size scales down with the square root of the film thickness, so that nanometer-sized domains are expected for ferroelectric tunnel barriers (which are typically thinner than 5 nm) [63]. Most recently, Xue *et al.* demonstrated ferroelectric switching in planar van der Waals α - In_2Se_3 memristors. They utilize interfacial engineering to modulate the Schottky barrier height and switching polarization at the ferroelectric material-electrode terminals and report a high *on*:*off* ratio of 10^4 in ferroelectric memristors [65].

5. Memristor devices based on halide perovskites

Various materials, such as metal oxides, polymers, chalcogens, and amorphous silicon, have been proposed to construct memristor devices, of which metal oxides have been widely studied; however, metal-oxide-based RS requires a complicated fabrication process and high power consumption. The HP gives the impression of being the most promising material compared to other materials because of a high *I-V* hysteresis, which facilitates ion migration, cost efficiency, defect tolerance, and flexibility in composition to tune the structural, optical, and electrical properties, providing an additional advantage in RS and artificial synaptic devices [20,36,48].

A HP-based memristive device was reported in 2015 by Yoo *et al.* In this work, the RS characteristic is demonstrated for the $Au/CH_3NH_3PbI_{3-x}Cl_x$/fluorine-doped indium tin oxide (FTO) device. The fabricated device exhibits bipolar RS with low set and reset voltages (0.8 and -0.6 V). The device achieves stable endurance

(>100 times) and a long retention time ($>10^4$ s) comparable to that of typical oxide-based devices, although the switching ratio of the device remains very low (<10) [66]. One of the critical issues for perovskites is their instability under ambient conditions. To address this issue, in 2016, Muthu *et al.* demonstrated a device based on 3D HP nanoparticles capped with octylammonium and having a structure of $FTO/MAPbBr_{3-x}Cl_x/Ag$. The device exhibits a switching ratio of 5×10^2 with an endurance of 250 cycles. In addition, the set-reset voltage decreases when the Cl content is increased in the perovskite structure because, with an increase in Cl content, the HP band gap decreases [67]. In the following year, Hwang *et al.* fabricated a memristive device with a structure of $Au/CH_3NH_3PbI_{3-x}Br_x/ITO$. As the Br quantity increases, with a value of $x = 0$, 1, 2, and 3, the HP film gradually changes color from semitransparent dark brown to light brown to yellow. As the Br content increases, the absorption band in the HP film shifts to shorter wavelengths. The study demonstrates that the energy band gap can be modulated by controlling the composition in HP. Also, with an increase in Br content, the set voltage of the device shows a decrease, leading to overall reduced power consumption. The device exhibits a switching ratio of 10^2 with a retention time of 2×10^4 s [68].

Despite having multiple advantages, 3D HP-based devices have a downside when it comes to stability. They can react with moisture and air, causing degradation of the device, and the degradation is enhanced with heat [15]. On the other hand, two-dimensional (2D) HP-based devices have distinct crystal structures compared to their 3D counterparts, and their dimensionality is not thickness dependent. The 2D perovskite-based devices exhibit certain superior properties over 3D perovskite-based devices. They consume ultralow power in both set and reset operations, exhibiting a low operating current. Compared to 3D HP-based devices, 2D HP-based devices show negligible leakage current and negligible HRS current due to reduced conductivity, as they exhibit high stability and hydrophobicity. Hence, the excellent properties of 2D perovskite make it viable for a wide range of applications in RS [16,37,38,69,70].

In 2020, Xia *et al.* fabricated a 3D HP-based RS device with a structure of $Al/MAPbI_{3-x}Cl_x/ITO$ in which voltage is applied to Al and ITO is earthed. The fabricated device exhibits RS with a meagre switching ratio (<10), exhibiting similar performance to that of the work done by Yoo *et al.* [70]. Then, by replacing the methylammonium ion in 3D HP with a long-chain organic cation, the authors developed a thin 2D HP layer over the 3D HP layer. The 2D or 3D heterostructure forms passivated defects of 3D HP. The engineered device has a structure of $Al/2D\ HP/MAPbI_{3-x}Cl_x/ITO$. The 2D or 3D HP-based device demonstrates a high switching ratio of 10^3. The devices also exhibit stable endurance (>300 cycles) with a

retention time of 10^4 s [70]. This experiment clearly indicates the magnificent properties of 2D HP that are favorable for the memristive device. To enhance HP-based RS device stability, in 2020, Kim *et al.* fabricated a memristor based on a quasi-2D HP. The RRAM device with a structure of Ag/(PEA)$_2$Cs$_3$Pb$_4$I$_{13}$/Pt (where PEA is Phenethylammonium) shows enhanced stability. It also leads to morphological improvements and a very high *on:off* ratio in the order of 10^9 [71]. Also, lead-based HP displays excellent characteristics, such as an easy fabrication strategy, long carrier-diffusion length, and a high amount of charge carriers. Several lead-HP-based RS devices exhibit remarkable performances; however, organic cations in the lead HP cause hygroscopicity, leading to device degradation. In addition, lead-based HP is very toxic for humans and the environment, which cannot be overlooked. Hence, despite having multiple advantages, lead-HP RS devices have limited practical implementation [39]. In 2019, Qian *et al.* fabricated a lead-free 3D HP MASnBr$_3$-based memristor with an ITO/MASnBr$_3$/Au device structure [20]. The device displays bipolar RS characteristics at set and reset voltages of (0.65 ± 0.15) and (-3.1 ± 0.6) V, respectively, along with a switching ratio ranging from 10^2 to 10^3. The devices exhibit a retention time of 10^4 s and endure for 10^4 cycles. The fabricated device retains its properties after being bent 1000 times with a radius curvature of 7.84 mm. In 2020, Kim *et al.* fabricated a RS device using a 2D copper-based HP [(BzA)$_2$CuBr$_4$] (where BzA is Benzylammonium) with a configuration of Ag/PMMA/(BzA)$_2$CuBr$_4$/Pt. A thin layer of PMMA is added to prevent the HP layer from undergoing a chemical reaction with the TE, moisture, or atmospheric oxygen. The device is driven by the ECM mechanism, and it demonstrates a very high RS of 10^8 on the millivolt scale. It also displays a high endurance of 2000 cycles and multilevel RS characteristics [72].

Additionally, the excessive roughness, insufficient coverage, and pinholes generated due to solution processing in halide-perovskite thin films can also cause the crossbar memristor devices to be short-circuited. Therefore, the perovskite films must be smooth, uniform, and compact; the electrodes need to be small and compact for efficient energy storage in perovskite memristors [45]. At present, a wide range of studies have been reported for long-term stabilities in perovskite materials; also, with optimization of the dimensionality and composition, the device stability can be enhanced [73]. Recently, we reported a thiocyanate-passivated diaminonaphthalene-incorporated Dion–Jacobson-phase 2D perovskite for highly efficient photovoltaic devices with a significant increase in device stability [74]. Also, in comparison with the solution process, the vapor-deposition method can be used to fabricate uniform and smooth thin films with controlled thickness to effectively produce equally efficient unit cells in a single-perovskite memristor. Subsequently, a one-diode–one-resistance (1D-1R) scheme was also adopted to decrease cross-talk interference in a crossbar array in perovskite memristors. Recently, Kang *et al.* fabricated a crossbar-array memristor device with the Au/MAPbI$_3$/Au structure that showed unipolar resistive behavior with a high *on:off* ratio of 10^8. They fabricate the perovskite active layer by using lead acetate precursors through a one-step solution-deposition method to induce fast crystallization and fabricate a pinhole-free smooth perovskite film. Furthermore, they utilize the 1D-1R scheme to fabricate electrodes in an 8×8 crossbar array structure [75].

III. ARTIFICIAL SYNAPSE AND NEUROMORPHIC COMPUTING BASED ON HALIDE-PEROVSKITE MEMRISTORS

Many efforts have been made to apply memory devices to neuromorphic computing by utilizing artificial synapses to emulate the function of the human brain. Some of the features of an artificial synapse, such as the materials and device structure, the signals used for stimulus, the simulated synaptic behavior, and the consumption of energy, need to be considered to realize the simulation of a biological synapse. Artificial synaptic devices can be configured in a two-terminal or three-terminal structure. These devices can be stimulated using an electronic signal, a photonic signal, or a combination of both. The external stimulus is used to simulate various typical synaptic plasticity functions. The light-stimulated device has multiple benefits over electrically stimulated devices, such as broader bandwidth, low cross talk, and better scalability, which can enhance computational speed in a neural network. The 2D HP's optical properties and wavelength can easily be manipulated by adjusting the composition during the synthesis process and such phenomena have not been reported in any other material. Hence, light-stimulated synaptic devices based on 2D HP show higher selectivity than an electrically stimulated device. Figure 3(a) illustrates a cross-section image of a two-terminal synaptic device, Fig. 3(b) shows the light-induced three-terminal memristor, and Fig. 3(c) presents a schematic diagram of a multiple-light-stimulated synapse based on HP.

Neuromorphic computing emulates the human brain and its functionality. Neuromorphic computing consists of an electronic neural network that can achieve a high degree of parallelism with a physically united memory and information-processing unit. Artificial synapses and synaptic plasticity are fundamental functional units in neuromorphic computing. Synaptic plasticity is obtained by fabricating a device based on a metal TE-HP-BE, where TE and BE act as pre- and postneurons and the HP layer acts like a synapse. The mechanism of an artificial synapse is based on ion migration and the trapping effect. When
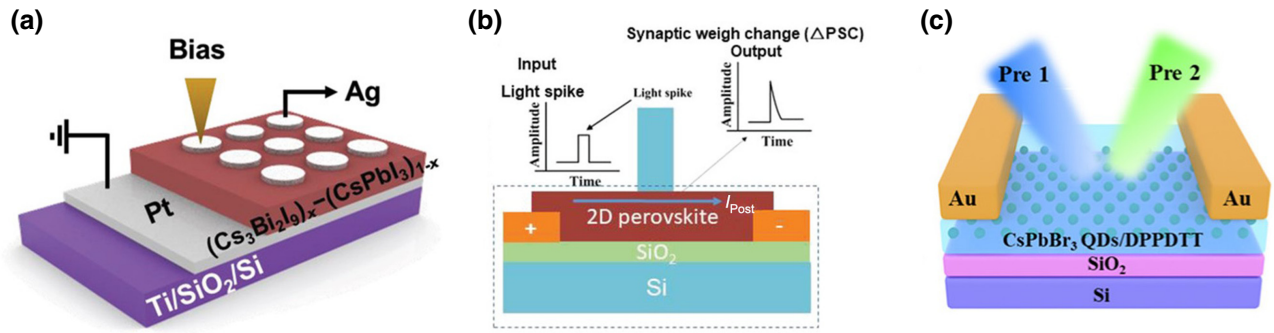
FIG. 3. (a) Two-terminal synaptic device where Ag mimics preneurons, Pt mimics postneurons, and the perovskite layer mimics a synapse. Reproduced with permission from Ref. [76]. Copyright 2019 John Wiley and Sons. (b) Cross-section image of a three-terminal light-induced synaptic device. Reproduced with permission from Ref. [38]. Copyright 2019 John Wiley and Sons. (c) Schematic diagram of a multiple-light-stimulated synapse based on HP. Reprinted with permission from Ref. [77]. Copyright (2020) American Chemical Society.

electrical stimuli are transmitted from preneuron to postneurons, there is a change in conductance termed as a change in synaptic weight (Δw). The synaptic weight can be represented as

$$\Delta w = (I_2 - I_1)/I_1, \tag{1}$$

where I_2 and I_1 are the postsynaptic current and presynaptic current, respectively.

When a low-frequency or small-amplitude pulse is applied, the synaptic weight changes sharply in the device, but it is very short lived, the process is called STP; however, when high amplitude or frequency is applied, a stable conductance path is formed, causing LTP. Short-term changes in synaptic weight occur in the range of milliseconds to minutes, and long-term changes in the device are related to memory and learning processes [36,48,76]. Short-term-memory (STM) and long-term-memory (LTM) behavior of the device is explained graphically in Figs. 4(a) and 4(b) [38]. STP and LTP behavior of the device is comparable to the human brain, i.e., when a stimulus registers sensory memory, the generated STM decays rapidly; however, by rapid rehearsal, STM is converted into LTM. These behaviors of the device can be controlled by controlling the supply of electric or light stimulus [38,76]. However, there are multiple parameters and factors that affect the effectiveness of synaptic devices, such as:

(a) STP [short-term depression (STD)]. The process of transient enhancement (reduction) of synaptic transmission in the neural system is known as STP (STD). It is generally believed that STP (STD) is related to the recognition and processing of external signals by the human brain. Biochemical changes in neurons are mainly responsible for this type of synaptic plasticity and recognized information is easily forgotten.

(b) PPF. Paired-pulse facilitation is a well-known form of STP. When two stimuli are delivered within a short

interval of time, and an enhanced response is observed for the second stimulus compared to the first stimulus, it is termed as PPF. Therefore, in terms of an artificial synapse, PPF is when the time duration between two consecutive pulses applied to the device is smaller than the recombination rate. A postsynaptic current (PSC) generated by a spike may exceed the current generated by a preceding spike. The PPF efficiency (η_{PPF}) of a device can be measured by

$$(\eta_{PPF}) = (A_2/A_1) \times 100\%, \tag{2}$$

$$(\eta_{PPF}) = [(A_2 - A_1)/A_1] \times 100\%. \tag{3}$$

Here, A_2 and A_1 signify the magnitude of ΔPSC activated by the second and first spike. The PPF mechanism for a neuromorphic computing-based device is illustrated in Fig. 4(c) [38,76,77].

(c) LTP [long-term depression (LTD)]. The process involving the persistent strengthening of synapses that leads to a long-lasting increase (decrease) in signal transmission between neurons is known as LTP (LTD). It is an important process in the context of synaptic plasticity. LTP (LTD) is related to learning and memory in the human brain. This type of synaptic plasticity generally includes changes in gene expression and structure; the memory of external information can last longer, such as for several months.

(d) STDP refers to a change in synaptic weight that is dependent on presynaptic and postsynaptic spikes. It depends on the interval of external signal pulses and the sequence that arrives at the synapse (presynaptic and postsynaptic terminals). When the time sequence changes for signals arriving at the synapse and if the synapse weight changes from potentiation (depression) to depression (potentiation), it is termed as asymmetric STDP,
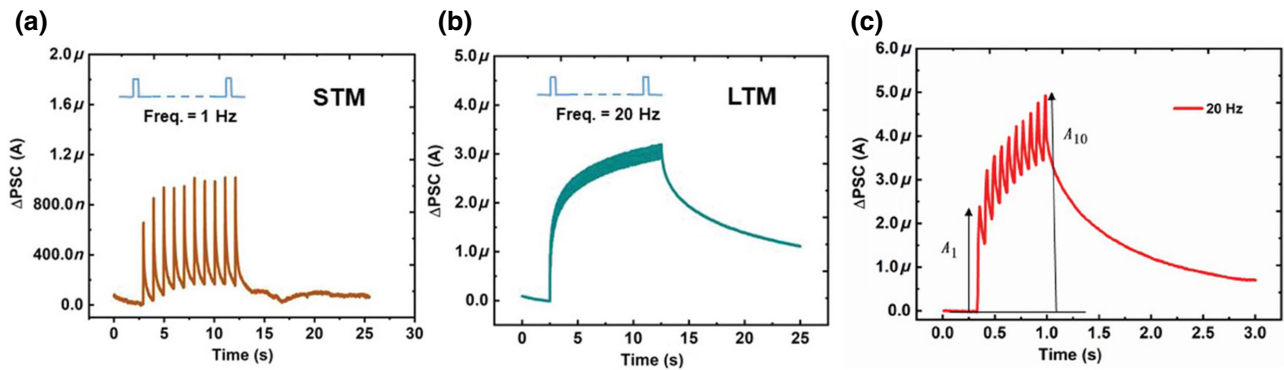
FIG. 4.　(a) STM and (b) LTM behavior of a synaptic device induced by stimuli of low and high frequency. (c) Postsynaptic current increases when 10 pulses are applied consecutively, exemplifying PPF mechanism. (a)–(c) Reproduced with permission from Ref. [38]. Copyright 2019 John Wiley and Sons.

otherwise it is termed as symmetric STDP. STDP is considered to be the most important learning mechanism of Hebbian theory and plays an important role in memory, learning, and information coding [76].

(e) Spike-duration-dependent plasticity (SDDP). SDDP refers to the change in PSC driven by the duration of the light or electric pulse applied to the device.

(f) Spike-number-dependent plasticity (SNDP). SNDP refers to the magnitude of the PSC value depending upon the number of light or electric pulses applied to device, i.e., when a higher number of pulses are applied, the device displays a higher PSC value.

(g) SRDP. The change in synaptic plasticity associated with the change in synaptic weight influenced by the spike rate or frequency is known as SRDP. The learning process of the device depends upon SRDP. When a high-frequency presynaptic pulse is applied, potentiation occurs, and when a low pulse is applied, depression occurs [36]. This type of synaptic plasticity is one of the most important synaptic functions in the cognitive behavior of the brain.

(h) EPSC [inhibitory postsynaptic current (IPSC)]. Excited by electrical or light stimuli, the preneuron releases excitatory (prohibiting) neurotransmitters into the synaptic cleft. These neurotransmitters are then received in the postsynaptic membrane and the excitatory (inhibitory) current is produced in the postsynaptic membrane through ion-flow regulation. This current produced in the postsynaptic membrane is known as EPSC (IPSC).

A. Two-terminal synaptic devices for neuromorphic computing and artificial synapses

Organometal halide perovskites are intensively studied as the resistive-switching layer in artificial synapses for the ultralow power consumption they can achieve. In 2016, Xiao and Huang reported a two-terminal synaptic device based on polycrystalline $MAPbI_3$ that mimicked the neuromorphic processes of learning and remembering with a

low power consumption of 55 fJ/(100 nm)^2·per spike compared to other anion-migration devices [78]. Many of the biological synapse functions are observed in the HP synaptic device, including four forms of STDP, SRDP, STP, LTP, and learning-experience behavior. Notably, the time constant of the synaptic function of HP-based synaptic devices for different STDP forms are about 80–300 ms, comparable to biological synapses. After poling with a long interval of 20.1-s voltage spikes, an almost unchanged read-out current density of 5.5×10^{-3} mA cm^{-2} is observed, which is the STP function. On the other hand, after poling with the short interval of 1.5-s voltage spikes, the dark current increases to 4.9×10^{-2} mA cm^{-2}, which is the LTP function. Photoread synaptic functions are also enabled due to the photovoltaic properties of the perovskite device. In addition, a very low energy consumption of fJ/(100 nm)^2 per event is shown, which is close to the energy consumption of biological synapses. This low energy consumption is attributed to the low activation energy of ion migration in the HP and switchable *p-i-n* structure. They also observe a read-out method where light is used in addition to an electric pulse as the stimulus.

In 2017, Tian *et al.* demonstrated a 2D-HP based memristor. An ultrathin exfoliated single crystal of 2D $(PEA)_2PbBr_4$ is obtained via monolayer step exfoliation. Here, the 2D HP is sandwiched between graphene and Au. To measure the RS properties in the structure of graphene/2D $(PEA)_2PbBr_4$/Au, graphene is earthed, and a voltage is applied to Au. Since a single crystal has no influence from grain boundaries, compared with 3D polycrystalline HP, they observed the set current to be very low (around 10 pA), 400 fj per synaptic operation, which is analogous to the human synapse energy consumption of 1–100 fj per synaptic event and very intriguing for neuromorphic electronics applications [37]. In 2018, Kumar *et al.* fabricated a RS device with a structure of $NiO_x/(C_4H_9NH_3)_2PbBr_4$/ZnO. The device exhibits bipolar RS at set and reset voltages of 1.2 and -2 V.

Due to the high band gap of the HP (3.0 eV), the device exhibits a high visible transmittance of 75%, opening up the possibility for transparent devices. The current transient behavior shows that the current values corresponding to a fixed voltage increase for successive pulses (showing the PPF mechanism), bringing up enormous possibilities in neuromorphic computing for the device [69]. From these two reports, it is clear that 2D halide perovskites have the capability to be used for artificial synapses, more functions of synaptic behaviors, such as STDP, SRDP, STD, and LTD, with 2D perovskite-based devices need to be examined. In 2019, Kim *et al.* fabricated a dual-phase two-terminal synaptic device based on all-inorganic HPs (IHPs). Researchers generated a uniform mixture of 2D $Cs_3Bi_2I_9$ and 3D $CsPbI_3$ phases. The fabricated device had a structure of $Ag/PMMA/(Cs_3Bi_2I_9)_{0.4}$-$(CsPbI_3)_{0.6}/Pt/Ti/SiO_2/Si$. The device exhibited a switching ratio of 3.2×10^8 with an endurance cycle of 1300 and retained data for 10^4 s. The device successfully mimicked multiple human brain functions, such as STP, LTP, conversion between STP and LTP, and STDP [76]. The synaptic STP and LTP are explored with 2 and 5 pulses of 0.1 V (640 μs), respectively. To determine the retention current, read-voltage pulses of 0.02 V are applied at 10-s intervals. After receiving the two programming pulses (0.1 V, 640 μs), the device shows an increase in the current level to about 10^{-7} A and is maintained for up to 20 s, then the current is abruptly decreased to the initial high-resistance state. This result represents the STP behavior of the IHP-based artificial synapse. The current level is switched to about 10^{-3} A and retained for up to 6000 s when five pulses (0.1 V, 640 μs) are applied to the device, indicating LTP behavior.

In the following year, Zeng *et al.* demonstrated a device based on a Cu-based HP. A Cu-based HP, such as $Cs_3Cu_2X_5$ ($X = $ Cl, I, Br) or $CsCu2X3$, exhibited high band gaps, stable crystal structures, excellent optical properties, and low toxicity. The fabricated device has a structure of $Ag/PMMA/Cs_3Cu_2I_5/ITO$. It displays a set-reset voltage much smaller than ± 1 V and a switching ratio of 10^2, with an endurance of 100 cycles and retention timing of $> 10^4$ s. The device emulates the human brain's synaptic functions, such as LTP and LTD. Based on this device, a classical multilayer perceptron neural network is constructed that can recognize handwritten numbers from the Modified National Institute of Standards and Technology (MNIST) data set. The hardware neural networks used here for handwritten data set recognition can recognized data with 94% accuracy [39].

Yang *et al.* fabricated a $CsPbCl_3$-based photonic synaptic device [79]. $CsPbCl_3$ exhibits sensitivity towards UV light and is highly stable. Researchers found that UV light enhanced the cognitive activities of the human brain related to memory, despite not being detected by the human retina. The fabricated device has a structure of $ITO/SnO_2/CsPbCl_3/TAPC/TAPC:MoO_3/MoO_3/Ag/MoO_3$ (where TAPC is 4,4′-Cyclohexylidenebis[N,N-bis(4-methylphenyl)benzenamine]). It is observed that the PSC is higher when a high-intensity light pulse illuminates the device. The fabricated device also demonstrates a highly sensitive photoresponse, even under weak illumination in the presence of UV light. The device demonstrates a different photoresponse under different light environments. In the presence of red illumination, it does not exhibit memory capability while, under UV-light illumination, the device exhibits long-term memory. The synaptic device also displays neuromorphic behaviors like STP, LTP, PPF, STDP, SNDP, and SDDP. The neuromorphic characteristics that are induced by ultraviolet light are attributed to carrier trapping and detrapping in the SnO_2 nanoparticles and $CsPbCl_3$ perovskite interface. These illustrative synaptic functions are shown in Fig. 5. The ratio of two PSCs, A_2/A_1, referred as the PPF index, is shown in Fig. 5(a). Figure 5(b) shows the photoresponses for ten consecutive pulses with spike intervals of 10 s clearly exhibiting PPF behavior. Figure 5(c) shows the function of SDDP with a PPF index of 126% when the spike duration is 0.5 s, and as the pulse period extends to 8 s, the PPF index decreases to 101%. Also, the spike frequency, spike-frequency-dependent plasticity (SFDP), is measured as the maximum SFDP index after ten spikes reach a considerably high value of 682.9% under light illumination of 12.5 μW cm^{-2}.

Gong *et al.* grew $MAPbBr_3$ single-crystalline thin platelets (SCTPs) using a thickness-confined surfactant-assistant self-assembly strategy. Then, a two-terminal lateral-structured synaptic device was fabricated that showed an ultralow operating current down to sub-pA [80]. Application of a presynaptic spike (PSS, –0.3 V, 906 ms) on one electrode of the SCTP-based synaptic devices results in the observation of EPSC through the other electrode under a small bias of –0.02 V. When the PSS arrives, the EPSC increases sharply to –0.57 pA and after the spike it decreases gradually. On application of a positive PSS, an inhibitory PSC is observed, decreasing to –0.29 pA. This may be ascribed to ion migration in perovskites driven by an electric field. The ultralow operating current is attributed to the absence of defect-mediated leakage paths. Different plasticity, such as spike-voltage-dependent plasticity, SDDP, SNDP, and SFDP, are also demonstrated for SCTP-based devices. In addition, synaptic functionality, including EPSC, IPSC, PPF, sensory memory to STM transition, potentiation-depression, and activity-dependent plasticity, are also demonstrated.

In 2021, Lao *et al.* fabricated a memristive artificial synaptic device with a lead-free double perovskite having the structure of $Ag/PMMA/Cs_2AgBiBr_6/ITO$ [81]. The RS mechanism is achieved at a deficient voltage supply of ± 0.5 V with an endurance of 110 cycles, switching ratio
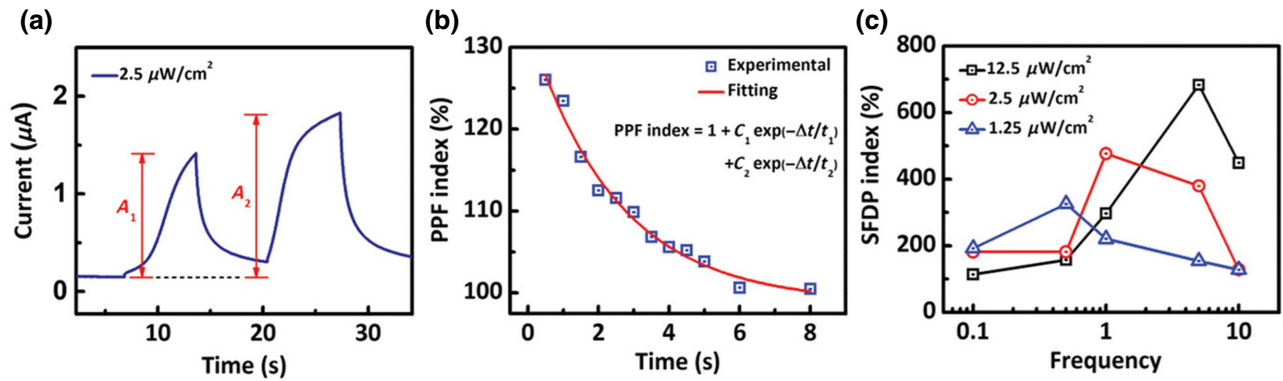
FIG. 5. (a) Postsynaptic current responses A_1 and A_2 versus time under 2.5 μW cm^{-2}. (b) PPF index plotted as a function of spike interval. (c) SFDP index illustrated as a function of frequency; range of frequency is between 0.1 and 10 Hz. (a)–(c) Reproduced with permission from Ref. [79]. Copyright 2021 John Wiley and Sons.

of 10, and retention time of 10^3 s. The fabricated device exhibits greater stability than that of organometallic-halide-perovskite-based devices. The device also demonstrates synaptic behaviors like EPSC, STP, LTP, PPF, and SRDP. The devices are then used for pattern recognition. An artificial neural network is built and connected through two synaptic weight arrays. The fabricated device demonstrates image recognition with 91.3% of accuracy.

In another report, Das *et al.* demonstrated two-terminal artificial synaptic devices having the structure Al/FAPbBr$_3$/ITO [82]. The device exhibits synaptic behavior like STP, LTP, PPF, EPSC, and STDP. The fabricated device consumes about 62.4 pJ of energy per synaptic event. They also studied the effect of light exposure on synaptic plasticity. EPSC is measured in the presence of UV light and in dark mode. The results reveal that the EPSC value is higher in the presence of UV compared with that in the dark mode. The change in the EPSC value under illumination can be attributed to the excellent optoelectronic properties of the HP film.

B. Three-terminal synaptic devices for neuromorphic computing and artificial synapses

Devices based on three terminals have a transistor structure and enhanced properties. A two-terminal device can achieve primary synaptic functions; however, signal transmission and learning cannot be performed simultaneously. In three-terminal devices, the gate electrode acts as a presynaptic membrane and a conducting channel acts a postsynaptic membrane. The structure of a three-terminal device can also be expanded to a multiterminal device, processing and simulating a large amount of data in parallel. The three-terminal device exhibits a high degree of flexibility in synaptic weight. It has a vast application potential in an artificial neural network; however, it has a complex structure that is difficult to fabricate on a large scale [36].

Although excellent performance is achieved in MAPbI$_3$-based photonic synapses, the toxicity of lead is a major concern, so designing green devices based on lead-free perovskites is an urgent requirement. In 2019, Sun *et al.* assembled an air-stable lead-free 2D (PEA)$_2$SnI$_4$-perovskite-based synaptic device signaled by light. It is observed that the presynaptic current increases rapidly under irradiation and returns to the initial value when the light source is removed. The device accomplishes PPF, short-term memory, long-term memory, and a short-term-to long-term-memory transition. STP and LTP are considered as the basic learning and memory mechanisms in neuroscience. A conversion from STP to LTP is achieved by applying light spikes of different frequencies with a fixed light irradiance of 11.6 μW cm^{-2}. When a series of light spikes with a period of 1 s and duration of 20 ms are applied, the postsynaptic current is quickly returned to its initial value. However, upon keeping the same irradiance and duration of light spikes but with high frequency (20 Hz), which can be seen as maintenance rehearsal, LTP behavior is observed [38]. In 2020, Hao *et al.* [77] developed a three-terminal light-induced synaptic device based on a HP-organic semiconductor. The fabricated device of DPPDTT (poly[2,5-(2-octyldodecyl)-3, 6-diketopyrrolopyrrole-alt-5,5-(2,5-di(thien-2-yl)thieno [3, 2-b]thiophene)])/CsPbBr$_3$ quantum dot (QD) PST is deposited on a heavily n-doped Si/SiO$_2$ substrate through spin coating. The device consumes ultralow electrical energy of 0.5 fJ/synapse and is stable under ambient conditions. It mimics various synaptic mechanisms like PPF, STM, and LTM. The device exhibits the capability to memorize images and emulate basic human-learning mechanisms, i.e., it takes 100 continuous pulses to excite the synaptic device, and when the pulse is withdrawn, the postsynaptic current subsides swiftly. Eventually, it took 22 consecutive pulses for the device to reach the previous learning level [77]. In the same year, Hong *et al.* fabricated a three-terminal synaptic device with a CsPb(Br$_{0.5}$I$_{0.5}$)$_3$-

MoS$_2$ hybrid structure fabricated on heavily *p*-doped Si/SiO$_2$ substrate. It can emulate the human eye's capability to transmute light energy into electrical energy based on the hybrid structure of the CsPb(Br$_{0.5}$I$_{0.5}$)$_3$ HP and MoS$_2$. The device exhibits selective degradation, which can be used for sensory-adaptation devices [83].

Recently, Shi *et al.* proposed a multifunctional synaptic device [84]. They utilize a ternary photosensitive layer based on an organic semiconductor (OSC) polymer-inorganic perovskite quantum dot (IPQD) to fabricate a high-performance dual-mode synaptic transistor. The synaptic device shows the lowest power consumption (∼0.11 fJ), owing to the dual optics-absorption functions of the OSCs and IPQDs along, with significant optically synapticlike behavior. The device also demonstrates tunable short-term and long-term neuroplasticity. The utilization of the polymer improves the stability and printability for the fabrication of printable devices. The different components of the ternary layer are chosen to cater for different functions. The C8-BTBT (2,7-Dioctyl[1]benzothieno[3,2-b][1]benzothiophene) OSC has a high-crystallinity function as a charge-transportation material with great UV responsivity, the IPQDs (CsPbBr$_3$ quantum dots) enhance UV absorption and charge transfer, and the polymer (polystyrene) functions as a charge-lifetime enhancer. STP and LTP are stimulated by an optical signal and the temporal and permanent changes to the current are achieved by changing the signal. Long-term stability (3×10^3 s), multilevel information-storage capability, and good switching stability are achieved in the synaptic device.

In addition, the Morse-code information-processing capability and pattern-recognition capability are also demonstrated by the synaptic transistor using a single-layer perception-based artificial neural network. Another report by Hao *et al.* demonstrates that a versatile heterojunction between perovskite nanocrystals (NCs) and semiconducting single-walled carbon nanotubes (SWCNTs) enables the neuromorphic functionality and memory property with very low energy consumption when stimulated optically [85]. This is achieved due to light-induced ion migration in the perovskite-nanocrystal-based heterojunctions. A room-temperature long-lived writable and erasable persistent photoconductivity (PPC) is achieved. Basic neuromorphic functions and optical switching are stimulated at low voltage with low energy per spiking event (femto- to picojoule energies). The PPC at the nanoscale interface of the nanocrystal array occurs due to field-assisted control of ion migration. The FET geometry (three-terminal device) gives the advantage of efficient lateral transport of carriers in the SWCNT channel along with out-of-plane electric field generation, which guides ion migration in the NC array for the realization of PPC. A comparison of important parameters of recent memristor and transistor-type devices used for artificial synapses is given in Table I.

1. Light-induced resistive switching in halide perovskites

Halide perovskites show a fast response to light illumination. Based on the photoresponse property, light-induced resistive switching is realized in several halide-perovskite memristors. Lin and co-workers fabricated a perovskite memristor based on photoresponsive properties with a device structure of ITO/PEDOT:PSS/MAPbI$_3$/Cu. The perovskite device exhibits outstanding electrically stable bipolar and nonvolatile rewritable memory effects with an excellent *on*:*off* ratio of 10^4 at a read-out voltage of 50 mV, a long retention time of up to 3×10^4 s, and 3000 endurance cycles. Subsequently, the perovskite device has shown outstanding photoresponsive behavior, with 10^{-6} mA cm^{-2} dark current and 10^{-3} mA cm^{-2} illumination current (under 100 mW cm^{-2} solar irradiance), and an *on*:*off* ratio (photoresponsive current) of 10^3. Consequently, by using the perovskite memristor, a photoinduced OR logic gate is also fabricated, which utilizes an electric field and light illumination as inputs *A* and *B*, and the current level as output *C*. Conclusively, the photoinduced perovskite memristor shows the capability of realizing logic disjunctions similar to a digital OR gate [87]. Similarly, Kim *et al.* fabricated a MAPbI$_3$-based RS device with an *on*:*off* ratio of 10^3, stable endurance, and a high retention of about 10^4 s. Moreover, the MAPbI$_3$ RS device exhibits multiresistance states at different intensities of light and can also be utilized in flexible wearable memory devices [88]. Furthermore, Zhou *et al.* also studied optoelectronic resistive switching and logic operations by using CH$_3$NH$_3$PbI$_{3-x}$Cl$_x$ perovskites with a device structure of FTO/CH$_3$NH$_3$PbI$_{3-x}$Cl$_x$/Au. The CH$_3$NH$_3$PbI$_{3-x}$Cl$_x$ cell exhibits an outstanding *on*:*off* ratio (∼10^3) at a low operating voltage of 0.1 V under light illumination, various resistance states, and long-term retention for over 400 endurance cycles. Its unique optoelectronic characteristics enable logic operations to be performed by inputting one electrical pulse and one optical signal and detecting the coincidence of the electrical and optical signals [89]. More recently, Zawal *et al.* incorporated a carbon nitride (C$_3$N$_4$) charge-trapping layer into traditional CH$_3$NH$_3$PbI$_3$ perovskites to fabricate photoresponsive perovskite memristors. They examined significant photocurrent enhancement and long-term plasticity in perovskite memristors after illumination under short light pulses (200 ms, 465 nm). They further claimed the fabrication of dual electrical and optical stimuli-based perovskite resistive-switching devices. Moreover, the charge-trapping characteristics of an additional C$_3$N$_4$ layer is largely responsible for different light-induced synaptic effects in perovskite memristors [51]. Also, Li *et al.*

TABLE I. Important parameters of recent memristors, transistor devices, and artificial synapses.

Structure	On:off ratio	V_{set} (V)	V_{reset} (V)	Endurance (cycle)	Retention time (s)	Energy per synapse	Ref.
ITO/CsCu$_2$I$_5$/PMMA/Ag	10^2	<1	>−1	100	>10^4	not available	[39]
ITO/Cs$_2$AgBiBr$_6$/PMMA/Ag	10	0.5	−0.5	110	10^3	188.6 pJ	[81]
FTO/NH$_3$PbI$_{3-x}$Cl$_x$/CH$_3$/Au	<10	0.8	−0.6	>100	>10^4	not available	[66]
FTO/MaPbBr$_{3-x}$Cl$_x$/Ag	5×10^2	not available	not available	250	not available	not available	[67]
ITO/CH$_3$NH$_3$PbI$_{3-x}$Br$_x$/Au	10^2	2	−2	not available	2×10	not available	[68]
ITO/MAPbI$_{3-x}$Cl$_x$/Al	>10	1.3	−1.3	3×10^2	10^4	not available	[70]
ITO/MaPbI$_{3-x}$Cl$_x$/2D HP/Al	10^3	0.79	−0.79	>300	10^4	not available	[70]
Pt/(PEA)$_2$Cs$_3$Pb$_4$I$_{13}$/Ag	10^9	0.18	−0.10	230	2000	not available	[71]
ITO/MASnBr$_3$/Au	10^2–10^3	0.65	−3.1	10^4	10^4	not available	[20]
Pt/(BzA)$_2$CuBr$_4$/PMMA/Ag	10^8	not available	not available	2000	not available	not available	[72]
Graphene/2D(PEA)$_2$PbBr$_4$/Au	10	2.8	not available	not available	10^3	400 fJ	[37]
NiO$_x$/(C$_4$H$_9$NH$_3$)$_2$PbBr$_4$/ZnO	not available	1.2	−2	not available	not available	not available	[69]
Pt/(CsBi$_2$I$_9$)$_{0.4}$-(CsPbI$_3$)$_{0.6}$/PMMA/Ag	3.2×10^8	not available	not available	1300	10^4	not available	[76]
ITO/FAPbBr$_3$/Al	not available	not available	not available	not available	not available	0.64 pJ	[82]
Si/SiO$_2$/DPPDTT/CsPbBr$_3$ QD PST/Au (SD)	not available	not available	not available	not available	>10^5	0.5 fJ	[77]
ITO/ALD Al$_2$O$_3$/C$_8$-BTBT/PS/CPB QDs/Au (SD)	not available	not available	not available	not available	3×10^3	0.11 fJ	[84]
Au/SWCNT-FAPbBr$_3$/Au	not available	not available	not available	not available	>10^3	<75 fJ	[85]
ITO/PEDOT:PSS/Ptpd/OGB capped CsPbBr$_3$/Ag	not available	1	−4	2×10^6	10^5	not available	[86]

fabricated Cs$_{0.15}$FA$_{0.85}$PbI$_{3-x}$Br$_x$-based nonvolatile optoelectronic memory devices and found that alternative resistance states could be switched in Cs$_{0.15}$FA$_{0.85}$PbI$_{3-x}$Br$_x$ memory devices with consecutive light and electrical input signals. The Cs$_{0.15}$FA$_{0.85}$PbI$_{3-x}$Br$_x$ memory devices show that light prompts an on:off ratio 10^2 and various logic operations can also be successfully realized by these devices [90].

In another report, Gong et al. demonstrated an artificial synapse in a MA halide-doped perovskite. A wider regulatory range of synaptic plasticity is achieved by improving the film morphology and crystallinity of FAPbI$_3$ perovskite through the introduction of MA halide additives [91]. The fundamental synaptic functions are conducted with

photoirradiation with a light intensity of 6.5 mW cm^{-2}. When a single spike of −1 V, 0.21 s, is applied on the top electrode, the doped perovskite-based device shows a larger EPSC response (−0.1 μA) and resting current than that of the pristine device due to the influence of the photogenerated current. The PPF behavior is also achieved by the application of two consecutive spikes (−1 V, 0.21 s) on the device. The second EPSC response is −0.19 μA, showing a distinct enhancement compared to the first response, suggesting that the doped device can lead to a stronger neural facilitation. High-order computing and learning behaviors are also realized with the help of photoirradiation, such as conditional reflex and logic operations. Moreover, the doped-perovskite artificial

synapse exhibits dynamic responses to environment changes. Therefore, it can be utilized to recognize environmental changes and to tune the information-processing efficiency.

2. Major differences between two-terminal and three-terminal devices

2T memristive synapse devices have recently shown unique advantages and are able to emulate some synaptic functions, such as STP (LTP), STDP, and triplet STDP. In addition, flexibility and transferability can also be achieved. Their structure is simple and can be fabricated with a high-density crossbar array architecture. However, the signal transmission and learning functions cannot be achieved simultaneously in 2T devices, so their ability to emulate a natural synapse is limited. On the other hand, 3T artificial synaptic devices have the merits of concurrently transmitting signals and performing learning. In a three-terminal transistor-type synaptic device, gate electrodes are typically treated as presynaptic terminals where an action potential is applied, and the channel layer with source-drain electrodes is considered to be equivalent to the postsynaptic membrane, whereas the channel conductance can be regulated by the presynaptic gate electrode. The dielectric layer is electrically insulating but ionically conductive, so it emulates the synaptic cleft to provide mobile ions, which migrate in response to presynaptic spikes. By application of a gate voltage, the conductance of the channel can be modulated. Therefore, 3T synaptic devices can receive and read stimuli concurrently. In addition, several gate electrodes can be used to obtain signals from multiple sources together, hence experiencing spatiotemporal effects, which cannot be achieved in 2T devices.

IV. CHALLENGES AND FUTURE OPPORTUNITIES

In conclusion, this review discusses recent advancements in HP-based memory devices and artificial synapses. HPs demonstrate intriguing electrical and optical properties compared to other materials, thus providing HPs with the multilevel modulation of the synaptic weight of artificial synapses, and hence, showing great potential in neuromorphic computing. With the development of HP-based memristors and other electrical devices in recent years, HP-based optically and electrically stimulated synaptic devices are accomplished successfully. To realize more complex synaptic functions, the development of artificial synapses based on HPs will mainly focus on three terminals or devices with more complex structures. The three-terminal devices exhibit many efficient properties compared to two-terminal devices, such as parallel learning and signal transmission. They can emulate human learning and sensory mechanisms and have huge

potential in artificial intelligence (AI) systems, AI sensors, and biomedical imaging. Three-terminal devices can be upgraded to multiterminal devices; this has yet to be achieved. Three-terminal devices have enormous possibilities that are yet to be explored. Hence, the future of memristive and neuromorphic computing devices is very much directed towards three-terminal devices.

Another challenge remaining is to develop devices with low energy consumption. To develop neuromorphic computing-based devices for practical implementation, the energy consumption per synaptic event needs to be reduced significantly. However, recent studies demonstrate a synaptic device that consumes 0.5 fJ per synaptic event, analogous to energy consumption by the human brain, (1–100) fJ/synapse. Yet, most of the fabricated devices consume much higher energy and further development in this direction is needed. The development of flexible memristive devices that can have applications in flexible and wearable electronics is another direction. Flexible neuromorphic electronics will allow artificial skin with senses such as feeling pain. Moreover, in terms of materials and integration, many challenges remains in neuromorphic systems, such as fabrication processes, linearity, device-to-device deviation, implementation of complex learning algorithms, and the sneak current in the crossbar array, also need to be overcome to achieve large-scale applications of artificial synapse technology.

[1] A. Miyata, A. Mitioglu, P. Plochocka, O. Portugall, J. T.-W. Wang, S. D. Stranks, H. J. Snaith, and R. J. Nicholas, Direct measurement of the exciton binding energy and effective masses for charge carriers in organic–inorganic tri-halide perovskites, Nat. Phys. **11**, 582 (2015).

[2] M. A. Afroz, N. Ghimire, K. M. Reza, B. Bahrami, R. S. Bobba, A. Gurung, A. H. Chowdhury, P. K. Iyer, and Q. Qiao, Thermal stability and performance enhancement of perovskite solar cells through oxalic acid-induced perovskite formation, ACS Appl. Energy Mater. **3**, 2432 (2020).

[3] C. C. Stoumpos and M. G. Kanatzidis, Halide perovskites: Poor man's high-performance semiconductors, Adv. Mater. **28**, 5778 (2016).

[4] M. A. Afroz, R. K. Gupta, R. Garai, M. Hossain, S. P. Tripathi, and P. K. Iyer, Crystallization and grain growth regulation through Lewis acid-base adduct formation in hot cast perovskite-based solar cells, Org. Electron. **74**, 172 (2019).

[5] M. A. Afroz, R. Garai, R. K. Gupta, and P. K. Iyer, Additive-assisted defect passivation for minimization of

open-circuit voltage loss and improved perovskite solar cell performance, ACS Appl. Energy Mater. **4,** 10468 (2021).

[6] J. Choi, J. S. Han, K. Hong, S. Y. Kim, and H. W. Jang, Organic–inorganic hybrid halide perovskites for memories, transistors, and artificial synapses, Adv. Mater. **30,** 1704002 (2018).

[7] J. Hu, L. Yan, and W. You, Two-dimensional organic–inorganic hybrid perovskites: A new platform for optoelectronic applications, Adv. Mater. **30,** 1802041 (2018).

[8] M. Manjappa, Y. K. Srivastava, A. Solanki, A. Kumar, T. C. Sum, and R. Singh, Hybrid lead halide perovskites for ultra-sensitive photoactive switching in terahertz metamaterial devices, Adv. Mater. **29,** 1605881 (2017).

[9] M. Ahmadi, T. Wu, and B. Hu, A review on organic–inorganic halide perovskite photodetectors: Device engineering and fundamental physics, Adv. Mater. **29,** 1605242 (2017).

[10] X. Guan, W. Hu, M. A. Haque, N. Wei, Z. Liu, A. Chen, and T. Wu, Light-responsive ion-redistribution-induced resistive switching in hybrid perovskite Schottky junctions, Adv. Funct. Mater. **28,** 1704665 (2018).

[11] Y. Shan, Z. Lyu, X. Guan, A. Younis, G. Yuan, J. Wang, S. Li, and T. Wu, Solution-processed resistive switching memory devices based on hybrid organic–inorganic materials and composites, Phys. Chem. Chem. Phys. **20,** 23837 (2018).

[12] W. Tress, Metal halide perovskites as mixed electronic–ionic conductors: Challenges and opportunities—from hysteresis to memristivity, J. Phys. Chem. Lett. **8,** 3106 (2017).

[13] D. W. deQuilettes, W. Zhang, V. M. Burlakov, D. J. Graham, T. Leijtens, A. Osherov, V. Bulović, H. J. Snaith, D. S. Ginger, and S. D. Stranks, Photo-induced halide redistribution in organic–inorganic perovskite films, Nat. Commun. **7,** 11683 (2016).

[14] G. Y. Kim, A. Senocrate, T.-Y. Yang, G. Gregori, M. Grätzel, and J. Maier, Large tunable photoeffect on ion conduction in halide perovskites and implications for photodecomposition, Nat. Mater. **17,** 445 (2018).

[15] S. Lee, H. Kim, D. H. Kim, W. B. Kim, J. M. Lee, J. Choi, H. Shin, G. S. Han, H. W. Jang, and H. S. Jung, Tailored 2d/3d halide perovskite heterointerface for substantially enhanced endurance in conducting bridge resistive switching memory, ACS Appl. Mater. Interfaces **12,** 17039 (2020).

[16] J. Zhang and W. Li, in *Perovskite Materials, Devices and Integration*, edited by H. Tian (IntechOpen, London, 2020).

[17] L. Chua, Memristor-The missing circuit element, IEEE Trans. Circuit Theory **18,** 507 (1971).

[18] N. D. Mathur, The fourth circuit element, Nature **455,** E13 (2008).

[19] D. B. Strukov, G. S. Snider, D. R. Stewart, and R. S. Williams, The missing memristor found, Nature **453,** 80 (2008).

[20] W.-H. Qian, X.-F. Cheng, J. Zhou, J.-H. He, H. Li, Q.-F. Xu, N.-J. Li, D.-Y. Chen, Z.-G. Yao, and J.-M. Lu, Lead-free perovskite MASnBr3-based memristor for quaternary information storage, InfoMat **2,** 743 (2020).

[21] A. Sawa, Resistive switching in transition metal oxides, Mater. Today **11,** 28 (2008).

[22] Z.-H. Tan, R. Yang, K. Terabe, X.-B. Yin, X.-D. Zhang, and X. Guo, Synaptic metaplasticity realized in oxide memristive devices, Adv. Mater. **28,** 377 (2016).

[23] F. Verbakel, S. C. J. Meskers, R. A. J. Janssen, H. L. Gomes, M. Cölle, M. Büchel, and D. M. d. Leeuw, Reproducible resistive switching in nonvolatile organic memories, Appl. Phys. Lett. **91,** 192103 (2007).

[24] Y. Yang, J. Ouyang, L. Ma, R. J.-H. Tseng, and C.-W. Chu, Electrical switching and bistability in organic/polymeric thin films and memory devices, Adv. Funct. Mater. **16,** 1001 (2006).

[25] R. N. Arunagirinathan, P. Gopikrishna, D. Das, and P. K. Iyer, Solution processed donor–acceptor polymer based electrical memory device with high on/off ratio and tunable properties, ACS Appl. Electron. Mater. **1,** 600 (2019).

[26] R. N. Arunagirinathan, N. Meher, and P. K. Iyer, Self-assembled naphthalimide nanoparticles for nonvolatile ReRAM devices: An efficient approach toward high performance solution-processed and all-organic two-terminal resistive memory devices, ACS Appl. Electron. Mater. **1,** 2437 (2019).

[27] Y. Li, Y. Zhong, L. Xu, J. Zhang, X. Xu, H. Sun, and X. Miao, Ultrafast synaptic events in a chalcogenide memristor, Sci. Rep. **3,** 1619 (2013).

[28] S. Yoo, T. Eom, T. Gwon, and C. S. Hwang, Bipolar resistive switching behavior of an amorphous $Ge_2Sb_2Te_5$ thin films with a Te layer, Nanoscale **7,** 6340 (2015).

[29] X. Zhao, H. Xu, Z. Wang, L. Zhang, J. Ma, and Y. Liu, Nonvolatile/volatile behaviors and quantized conductance observed in resistive switching memory based on amorphous carbon, Carbon **91,** 38 (2015).

[30] X. Zhao, H. Xu, Z. Wang, Z. Xu, C. Zhang, G. Wang, W. Liu, J. Ma, and Y. Liu, Sp^2 clustering-induced improvement of resistive switching uniformity in Cu/amorphous carbon/Pt electrochemical metallization memory, J. Mater. Chem. C **5,** 5420 (2017).

[31] S. H. Jo, K.-H. Kim, and W. Lu, High-density crossbar arrays based on a SI memristive system, Nano Lett. **9,** 870 (2009).

[32] Y. Yang, P. Gao, S. Gaba, T. Chang, X. Pan, and W. Lu, Observation of conducting filament growth in nanoscale resistive memories, Nat. Commun. **3,** 732 (2012).

[33] T.-Y. Yang, G. Gregori, N. Pellet, M. Grätzel, and J. Maier, The significance of ion conduction in a hybrid organic–inorganic lead-iodide-based perovskite photosensitizer, Angew. Chem., Int. Ed. **54,** 7905 (2015).

[34] J. Haruyama, K. Sodeyama, L. Han, and Y. Tateyama, First-principles study of ion diffusion in perovskite solar cell sensitizers, J. Am. Chem. Soc. **137,** 10048 (2015).

[35] X. Zhu, J. Lee, and W. D. Lu, Iodine vacancy redistribution in organic–inorganic halide perovskite films and resistive switching effects, Adv. Mater. **29,** 1700527 (2017).

[36] S. Chen and J. Huang, Recent advances in synaptic devices based on halide perovskite, ACS Appl. Electron. Mater. **2,** 1815 (2020).

[37] H. Tian, L. Zhao, X. Wang, Y.-W. Yeh, N. Yao, B. P. Rand, and T.-L. Ren, Extremely low operating current resistive memory based on exfoliated 2D perovskite single

crystals for neuromorphic computing, ACS Nano **11,** 12247 (2017).

[38] Y. Sun, L. Qian, D. Xie, Y. Lin, M. Sun, W. Li, L. Ding, T. Ren, and T. Palacios, Photoelectric synaptic plasticity realized by 2D perovskite, Adv. Funct. Mater. **29,** 1902538 (2019).

[39] F. Zeng, Y. Guo, W. Hu, Y. Tan, X. Zhang, J. Feng, and X. Tang, Opportunity of the lead-free all-inorganic $Cs_3Cu_2I_5$ perovskite film for memristor and neuromorphic computing applications, ACS Appl. Mater. Interfaces **12,** 23094 (2020).

[40] T.-C. Chang, K.-C. Chang, T.-M. Tsai, T.-J. Chu, and S. M. Sze, Resistance random access memory, Mater. Today **19,** 254 (2016).

[41] X. Hong, D. J. Loy, P. A. Dananjaya, F. Tan, C. Ng, and W. Lew, Oxide-based RRAM materials for neuromorphic computing, J. Mater. Sci. **53,** 8720 (2018).

[42] H. Bian, Y. Y. Goh, Y. Liu, H. Ling, L. Xie, and X. Liu, Stimuli-responsive memristive materials for artificial synapses and neuromorphic computing, Adv. Mater. **33,** 2006469 (2021).

[43] I. Raifuku, Y.-P. Chao, H.-H. Chen, C.-F. Lin, P.-E. Lin, L.-C. Shih, K.-T. Chen, J.-Y. Chen, J.-S. Chen, and P. Chen, Halide perovskite for low-power consumption neuromorphic devices, EcoMat **3,** e12142 (2021).

[44] H. Kim, J. S. Han, S. G. Kim, S. Y. Kim, and H. W. Jang, Halide perovskites for resistive random-access memories, J. Mater. Chem. C **7,** 5226 (2019).

[45] X. Xiao, J. Hu, S. Tang, K. Yan, B. Gao, H. Chen, and D. Zou, Recent advances in halide perovskite memristors: Materials, structures, mechanisms, and applications, Adv. Mater. Technol. **5,** 1900914 (2020).

[46] X. Zhao, Z. Wang, W. Li, S. Sun, H. Xu, P. Zhou, J. Xu, Y. Lin, and Y. Liu, Photoassisted electroforming method for reliable low-power organic–inorganic perovskite memristors, Adv. Funct. Mater. **30,** 1910151 (2020).

[47] B. Mohammad, M. A. Jaoude, V. Kumar, D. M. A. Homouz, H. A. Nahla, M. Al-Qutayri, and N. Christoforou, State of the art of metal oxide memristor devices, Nanotechnol. Rev. **5,** 311 (2016).

[48] Y. Huang, L. Tang, C. Wang, H. Fan, Z. Zhao, H. Wu, M. Xu, R. Shen, Y. Yang, and J. Bian, Triple-cation perovskite resistive switching memory with enhanced endurance and retention, ACS Appl. Electron. Mater. **2,** 3695 (2020).

[49] Z. Chen, Y. Yu, L. Jin, Y. Li, Q. Li, T. Li, Y. Zhang, H. Dai, and J. Yao, Artificial synapses with photoelectric plasticity and memory behaviors based on charge trapping memristive system, Mater. Des. **188,** 108415 (2020).

[50] D. S. Shang, L. Shi, J. R. Sun, B. G. Shen, F. Zhuge, R. W. Li, and Y. G. Zhao, Improvement of reproducible resistance switching in polycrystalline tungsten oxide films by in situ oxygen annealing, Appl. Phys. Lett. **96,** 072103 (2010).

[51] P. Zawal, T. Mazur, M. Lis, A. Chiolerio, and K. Szaciłowski, Light-induced synaptic effects controlled by incorporation of charge-trapping layer into hybrid perovskite memristor, Adv. Electron. Mater. **8,** 2100838 (2022).

[52] H. S. Majumdar, A. Bandyopadhyay, A. Bolognesi, and A. J. Pal, Memory device applications of a conjugated polymer: Role of space charges, J. Appl. Phys. **91,** 2433 (2002).

[53] D. Kuzum, R. G. D. Jeyasingh, B. Lee, and H. S. P. Wong, Nanoelectronic programmable synapses based on phase change materials for brain-inspired computing, Nano Lett. **12,** 2179 (2012).

[54] J.-J. Wang, Y.-Z. Xu, R. Mazzarello, M. Wuttig, and W. Zhang, A review on disorder-driven metal–insulator transition in crystalline vacancy-rich GeSbTe phase-change materials, Materials **10,** 862 (2017).

[55] M. Salinga, E. Carria, A. Kaldenbach, M. Bornhöfft, J. Benke, J. Mayer, and M. Wuttig, Measurement of crystal growth velocity in a melt-quenched phase-change material, Nat. Commun. **4,** 2371 (2013).

[56] A. Sebastian, M. Le Gallo, and D. Krebs, Crystal growth within a phase change memory cell, Nat. Commun. **5,** 4314 (2014).

[57] H. G. Kim, V. R. Nallagatla, D.-H. Kwon, C. U. Jung, and M. Kim, In situ observations of topotactic phase transitions in a ferrite memristor, J. Appl. Phys. **128,** 074501 (2020).

[58] M. R. Kiran, H. Ulla, Krishnamanohara, M. N. Satyanarayan, and G. Umesh, Observation of resistance switching in vanadyl-phthalocyanine thin films, Synth. Met. **269,** 116524 (2020).

[59] T. J. Whitcher, K. L. Woon, W. S. Wong, N. Chanlek, H. Nakajima, T. Saisopa, and P. Songsiriritthigul, Interfacial behavior of resistive switching in ITO–PVK–Al WORM memory devices, J. Phys. D **49,** 075104 (2016).

[60] T. F. Schranghamer, A. Oberoi, and S. Das, Graphene memristive synapses for high precision neuromorphic computing, Nat. Commun. **11,** 5474 (2020).

[61] S. Majumdar, H. Tan, Q. H. Qin, and S. van Dijken, Energy-efficient organic ferroelectric tunnel junction memristors for neuromorphic computing, Adv. Electron. Mater. **5,** 1800795 (2019).

[62] V. Mikheev, A. Chouprik, Y. Lebedinskii, S. Zarubin, Y. Matveyev, E. Kondratyuk, M. G. Kozodaev, A. M. Markeev, A. Zenkevich, and D. Negrov, Ferroelectric second-order memristor, ACS Appl. Mater. Interfaces **11,** 32108 (2019).

[63] A. Chanthbouala, V. Garcia, R. O. Cherifi, K. Bouzehouane, S. Fusil, X. Moya, S. Xavier, H. Yamada, C. Deranlot, N. D. Mathur, *et al.*, A ferroelectric memristor, Nat. Mater. **11,** 860 (2012).

[64] V. Mikheev, A. Chouprik, Y. Lebedinskii, S. Zarubin, A. M. Markeev, A. V. Zenkevich, and D. Negrov, Memristor with a ferroelectric HfO_2 layer: in which case it is a ferroelectric tunnel junction, Nanotechnology **31,** 215205 (2020).

[65] F. Xue, X. He, Y. Ma, D. Zheng, C. Zhang, L.-J. Li, J.-H. He, B. Yu, and X. Zhang, Unraveling the origin of ferroelectric resistance switching through the interfacial engineering of layered ferroelectric-metal junctions, Nat. Commun. **12,** 7291 (2021).

[66] E. J. Yoo, M. Lyu, J.-H. Yun, C. J. Kang, Y. J. Choi, and L. Wang, Resistive switching behavior in organic–inorganic hybrid $CH_3NH_3PbI_{3-x}Cl_x$ perovskite for resistive random access memory devices, Adv. Mater. **27,** 6170 (2015).

[67] C. Muthu, S. Agarwal, A. Vijayan, P. Hazra, K. B. Jinesh, and V. C. Nair, Hybrid perovskite nanoparticles for high-performance resistive random access memory devices: Control of operational parameters through chloride doping, Adv. Mater. Interfaces **3,** 1600092 (2016).

[68] B. Hwang, C. Gu, D. Lee, and J.-S. Lee, Effect of halide-mixing on the switching behaviors of organic-inorganic hybrid perovskite memory, Sci. Rep. **7,** 43794 (2017).

[69] M. Kumar, H.-S. Kim, D. Y. Park, M. S. Jeong, and J. Kim, Compliance-free multileveled resistive switching in a transparent 2D perovskite for neuromorphic computing, ACS Appl. Mater. Interfaces **10,** 12768 (2018).

[70] F. Xia, Y. Xu, B. Li, W. Hui, S. Zhang, L. Zhu, Y. Xia, Y. Chen, and W. Huang, Improved performance of $CH_3NH_3PbI_{3-x}Cl_x$ resistive switching memory by assembling 2D/3D perovskite heterostructures, ACS Appl. Mater. Interfaces **12,** 15439 (2020).

[71] H. Kim, M.-J. Choi, J. M. Suh, J. S. Han, S. G. Kim, Q. V. Le, S. Y. Kim, and H. W. Jang, Quasi-2D halide perovskites for resistive switching devices with on/off ratios above 109, NPG Asia Mater. **12,** 21 (2020).

[72] S.-Y. Kim, J.-M. Yang, E.-S. Choi, and N.-G. Park, Layered $(C_6H_5CH_2NH_3)_2CuBr_4$ perovskite for multilevel storage resistive switching memory, Adv. Funct. Mater. **30,** 2002653 (2020).

[73] C. Liu, M. Hu, X. Zhou, J. Wu, L. Zhang, W. Kong, X. Li, X. Zhao, S. Dai, B. Xu, *et al.*, Efficiency and stability enhancement of perovskite solar cells by introducing $CsPbI_3$ quantum dots as an interface engineering layer, NPG Asia Mater. **10,** 552 (2018).

[74] Yukta, R. D. Chavan, D. Prochowicz, P. Yadav, M. M. Tavakoli, and S. Satapathi, Thiocyanate-passivated diaminonaphthalene-incorporated Dion–Jacobson perovskite for highly efficient and stable solar cells, ACS Appl. Mater. Interfaces **14,** 850 (2022).

[75] K. Kang, H. Ahn, Y. Song, W. Lee, J. Kim, Y. Kim, D. Yoo, and T. Lee, High-performance solution-processed organometal halide perovskite unipolar resistive memory devices in a cross-bar array structure, Adv. Mater. **31,** 1804841 (2019).

[76] S. G. Kim, Q. Van Le, J. S. Han, H. Kim, M.-J. Choi, S. A. Lee, T. L. Kim, S. B. Kim, S. Y. Kim, and H. W. Jang, Dual-phase all-inorganic cesium halide perovskites for conducting-bridge memory-based artificial synapses, Adv. Funct. Mater. **29,** 1906686 (2019).

[77] D. Hao, J. Zhang, S. Dai, J. Zhang, and J. Huang, Perovskite/organic semiconductor-based photonic synaptic transistor for artificial visual system, ACS Appl. Mater. Interfaces **12,** 39487 (2020).

[78] Z. Xiao and J. Huang, Energy-efficient hybrid perovskite memristors and synaptic devices, Adv. Electron. Mater. **2,** 1600100 (2016).

[79] L. Yang, M. Singh, S.-W. Shen, K.-Y. Chih, S.-W. Liu, C.-I. Wu, C.-W. Chu, and H.-W. Lin, Transparent and flexible inorganic perovskite photonic artificial synapses with dual-mode operation, Adv. Funct. Mater. **31,** 2008259 (2021).

[80] J. Gong, H. Yu, X. Zhou, H. Wei, M. Ma, H. Han, S. Zhang, Y. Ni, Y. Li, and W. Xu, Lateral artificial synapses on hybrid perovskite platelets with modulated neuroplasticity, Adv. Funct. Mater. **30,** 2005413 (2020).

[81] J. Lao, W. Xu, C. Jiang, N. Zhong, B. Tian, H. Lin, C. Luo, J. Travas-sejdic, H. Peng, and C.-G. Duan, An air-stable artificial synapse based on a lead-free double perovskite $Cs_2AgBiBr_6$ film for neuromorphic computing, J. Mater. Chem. C **9,** 5706 (2021).

[82] U. Das, P. Sarkar, B. Paul, and A. Roy, Halide perovskite two-terminal analog memristor capable of photo-activated synaptic weight modulation for neuromorphic computing, Appl. Phys. Lett. **118,** 182103 (2021).

[83] S. Hong, S. H. Choi, J. Park, H. Yoo, J. Y. Oh, E. Hwang, D. H. Yoon, and S. Kim, Sensory adaptation and neuromorphic phototransistors based on $CsPb(Br_{1-x}I_x)_3$ perovskite and MoS_2 hybrid structure, ACS Nano **14,** 9796 (2020).

[84] Q. Shi, D. Liu, D. Hao, J. Zhang, L. Tian, L. Xiong, and J. Huang, Printable, ultralow-power ternary synaptic transistors for multifunctional information processing system, Nano Energy **87,** 106197 (2021).

[85] J. Hao, Y.-H. Kim, S. N. Habisreutinger, S. P. Harvey, E. M. Miller, S. M. Foradori, M. S. Arnold, Z. Song, Y. Yan, J. M. Luther, *et al.*, Low-energy room-temperature optical switching in mixed-dimensionality nanoscale perovskite heterojunctions, Sci. Adv. **7,** eabf1959 (2021).

[86] R. A. John, Y. Demirağ, Y. Shynkarenko, Y. Berezovska, N. Ohannessian, M. Payvand, P. Zeng, M. I. Bodnarchuk, F. Krumeich, G. Kara, *et al.*, Reconfigurable halide perovskite nanocrystal memristors for neuromorphic computing, Nat. Commun. **13,** 2074 (2022).

[87] G. Lin, Y. Lin, R. Cui, H. Huang, X. Guo, C. Li, J. Dong, X. Guo, and B. Sun, An organic–inorganic hybrid perovskite logic gate for better computing, J. Mater. Chem. C **3,** 10793 (2015).

[88] D. J. Kim, Y. J. Tak, W.-G. Kim, J. K. Kim, J. H. Kim, and H. J. Kim, Resistive switching properties through iodine migrations of a hybrid perovskite insulating layer, Adv. Mater. Interfaces **4,** 1601035 (2017).

[89] F. Zhou, Y. Liu, X. Shen, M. Wang, F. Yuan, and Y. Chai, Low-voltage, optoelectronic $CH_3NH_3PbI_{3-x}Cl_x$ memory with integrated sensing and logic operations, Adv. Funct. Mater. **28,** 1800080 (2018).

[90] Y. Li, P. Cheng, L. Zhou, Z. Liu, Z. Zuo, X. Zhan, and J. Chen, Light-induced nonvolatile resistive switching in $Cs_{0.15}FA_{0.85}PbI_{3-x}Br_x$ perovskite-based memristors, Solid State Electron. **186,** 108166 (2021).

[91] J. Gong, H. Wei, Y. Ni, S. Zhang, Y. Du, and W. Xu, Methylammonium halide-doped perovskite artificial synapse for light-assisted environmental perception and learning, Mater. Today Phys. **21,** 100540 (2021).